Accepted Manuscript

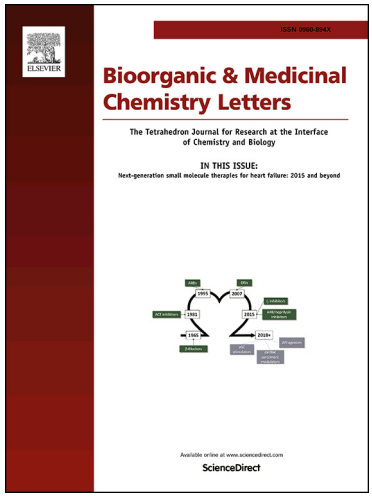

Novel, potent, selective, and brain penetrant phosphodiesterase 10A inhibitors

Hervé Geneste, Karla Drescher, Clarissa Jakob, Loïc Laplanche, Michael Ochse, Maricel Torrent

PII: S0960-894X(18)30976-4
DOI: https://doi.org/10.1016/j.bmcl.2018.12.029
Reference: BMCL 26198

To appear in: *Bioorganic & Medicinal Chemistry Letters*

Received Date: 6 November 2018
Revised Date: 12 December 2018
Accepted Date: 13 December 2018

Please cite this article as: Geneste, H., Drescher, K., Jakob, C., Laplanche, L., Ochse, M., Torrent, M., Novel, potent, selective, and brain penetrant phosphodiesterase 10A inhibitors, *Bioorganic & Medicinal Chemistry Letters* (2018), doi: https://doi.org/10.1016/j.bmcl.2018.12.029

Bioorganic & Medicinal Chemistry Letters
journal homepage: www.elsevier.com

Novel, potent, selective, and brain penetrant phosphodiesterase 10A inhibitors

Hervé Geneste,[a,*] Karla Drescher,[a,§] Clarissa Jakob,[b] Loïc Laplanche,[c] Michael Ochse,[a] Maricel Torrent,[b]

[a]*AbbVie Deutschland GmbH & Co. KG, Neuroscience Research, D-67008 Ludwigshafen, Germany;* [b]*AbbVie, Structural Biology, IL 60064-6101, U.S.A;* [c]*AbbVie Deutschland GmbH & Co. KG, DMPK, D-67008 Ludwigshafen, Germany.*

dedicated to the memory of Professor Jacques Coste, ENSC Montpellier, France

ARTICLE INFO

Article history:
Received
Revised
Accepted
Available online

Keywords:
phosphodiesterase
PDE10A
WEB-3

ABSTRACT

Herein we report the discovery of a novel series of phosphodiesterase 10A inhibitors. Optimization of a HTS hit (**17**) resulted in potent, selective, and brain penetrant **23** and **26**; both exhibited much lower clearance *in vivo* and decreased volume of distribution (rat PK) and have thus the potential to inhibit the PDE10A target *in vivo* at a lower efficacious dose than the reference compound WEB-3.

Inhibitors of phosphodiesterase 10A (PDE10A) offer a promising therapeutic approach for the treatment or prevention of neurological and psychiatric disorders, in particular schizophrenia and related disorders. Activity in several antipsychotic models has been shown with papaverine,[1] the first extensively profiled pharmacological tool compound for this target. These models suggest that PDE10A inhibition has the classical antipsychotic potential. Moreover inhibition of PDE10A reverses sub-chronic PCP-induced deficits in attentional set-shifting in rats suggesting that PDE10A inhibitors might alleviate cognitive deficits associated with schizophrenia.[2]

Identification and optimization of PDE10A inhibitors are highly supported by X-ray structures: three main binding modes are reported and illustrated in the literature[3] by papaverine, MP-10 and WEB-3. Most lead optimization programs targeting PDE10A inhibitors started either from papaverine[4] or from MP-10.[5] However in many cases PDE isoenzyme selectivity was a challenge. WEB-3,[6] out of the imidazo[1,5-a]-pyrido[3,2-e]pyrazine chemical series, depicted a novel binding mode into the PDE10A pocket. However its mutagenic potential (Ames positive) and its sub-optimal metabolic stability had to be addressed.[6]

As for most PDE10A inhibitors, H-bond interaction with Gln726 is critical.[3] In the case of WEB-3 (Fig. 1), additional interactions include water-mediated H-bonds with Tyr524 and Asp674 as well as π-stacking interactions with Phe729, Phe696 and Ile692 (hydrophobic clamp).[6]

In the past decade, multiple PDE10A inhibitors have been advanced to clinical trials for the treatment of neurological disorders and psychiatric diseases but none has yet reached the market.[7]

We present here the discovery of novel, selective and brain penetrant PDE10A inhibitors (Fig. 2) depicting a WEB-3-like binding mode. The new PDE10A inhibitors are PDE-selective,[8a] metabolically stable, Ames[8b] negative and cover a different CNS druglike space (clogP < 3, CNS MPO score ≥ 5.0) compared to formerly published related structural series.[9]

Two different approaches starting from WEB-3 were investigated to come to proprietary PDE10A inhibitors: the thiazolopyrazine[10] and cinnoline[11] structural series were thus identified (Fig. 1).

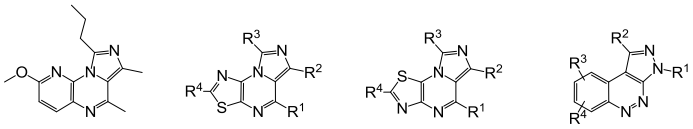

WEB-3[6] **I** **II** **III**

Figure 1. WEB-3[6] and AbbVie proprietary series (thiazolopyrazine (**I** & **II**) & cinnoline (**III**) derivatives)

*Corresponding author:
Tel.: +49-621-589-3423; e-mail: herve.geneste@abbvie.com

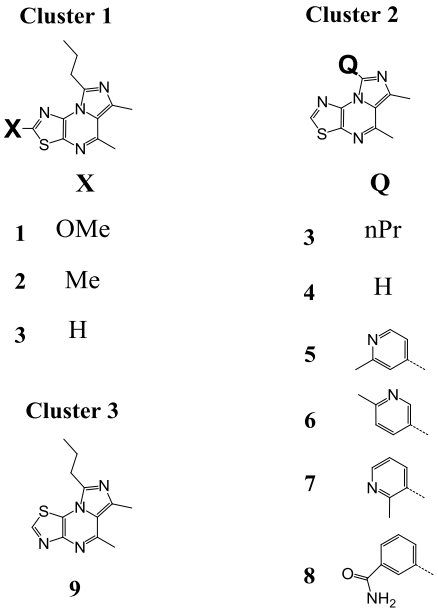

Figure 2. Thiazolopyrazine derivatives **1**-**9**

In our first approach the pyridine moiety of WEB-3 was replaced by a bioisosteric thiazole (**1**, Fig. 2). This single change was expected to impact the binding mode of the new tricyclic molecule (compared to WEB-3). Even in the most conservative scenario (namely, that the imidazolopyrazine portion of the core remains in a similar position, see Fig. 3), the OMe group of **1** (shown in salmon) would be redirected more towards residues Met703 and Tyr683 (shown in purple); this outcome would be slightly less favorable compared to what is observed for WEB-3 (cyan).[12]

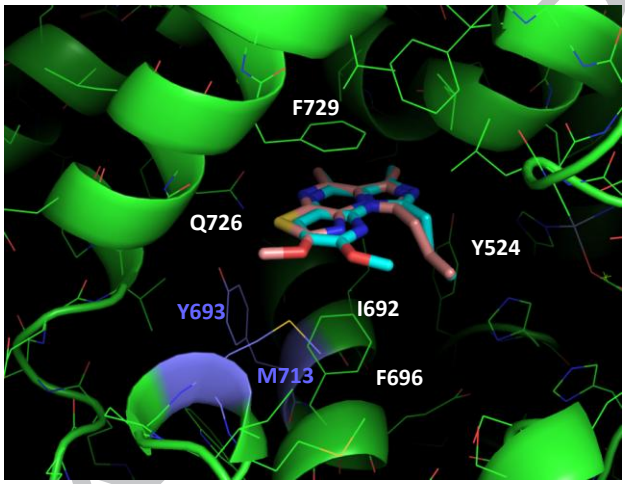

Figure 3. Comparison of **1** (model, salmon) docked into the PDE10A protein (green) and WEB-3 (X-ray PDB 3LXG, cyan) bound to the PDE10A binding site.[12] Notice the shift in binding and specific location of OMe tail.

Analogs **3**-**8** (Fig. 2, cluster 2) were prepared[10] starting from the commercially available thiazole-5-carboxylic acid **10**. The thiazole carbamate **11** obtained after Curtius rearrangement was deprotected, acetylated and finally brominated (**14**) after degradation of the dibrominated intermediate (not shown). The imidazole moiety was introduced by copper catalyzed coupling to afford **15**, which was then cyclized to form the tricyclic central core. Radical bromination yielded the halogenated precursor for the Suzuki coupling.

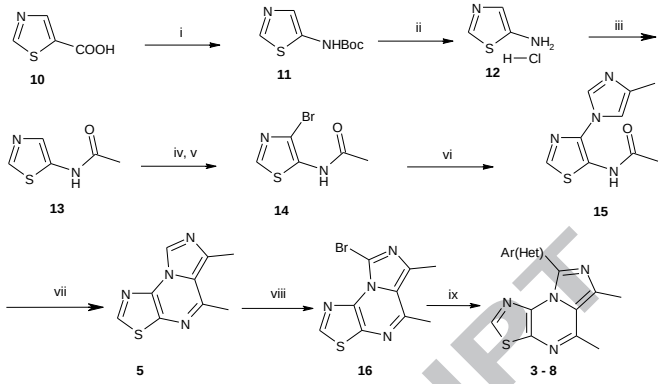

Scheme 1. Synthesis[10] of thiazolopyrazine derivatives; (i) DPPA, TEA, *t*-BuOH, 90°C, 12h, 40%; (ii) HCL/dioxane, MeOH, rt, 2h, 80%; (iii) Ac_2O, Et_3N, DCM, rt, 3h, 70%; (iv) Br_2, $CHCl_3$, rt, 12h, 66%; (v) Raney Ni, DEA, EtOH, rt, 12h, 78%; (vi) 4-methyl-1*H*-imidazole, (*1R*,*2R*)-N^1,N^2-dimethylcyclohexane-1,2-diamine, CuI, Cs_2CO_3, DMF, 90°C, 12h, 20%; (vii) P_2O_5/$POCl_3$, sealed tube, 160°C, 12h, 33%; (viii) NBS, CH_3CN, 20°C, 1h, 15%; (ix) (Het)ArB$(OH)_2$, $Pd(Ph_3P)_4$, $NaHCO_3$, PhMe/EtOH: 4/1, 100°C or $PdCl_2$(dppf), Cs_2CO_3, dioxane/H_2O: 4/1, 100°C.

Replacement of the pyridine moiety by a thiazole was accompanied by both a diminution of LLE[13] due to the reduced *in-vitro* potency (IC_{50}, 5-fold less compared to WEB-3; LLE 3.1) and higher lipophilicity (clogP 3.7 to 4.0 for **1**); the vector of the substituents off the thiazole is less optimal than the vector off the parent pyridine in WEB-3 (not shown). Me or H in place of the OMe substituent (on position 2) retained the same level of *in vitro* potency but allowed improved LLE (due to reduced clogP: 3.6 and 3.1 for **2** and **3** resp.; LLE 3.5 and 3.9 resp.), reduced TPSA (both 43 *vs* 52 for WEB-3) and higher permeability[14] (P_{app} 68-89 10E-6 cm/s, Table 1). In particular **3** depicted single digit microsomal stability (hmCl, Table 1) and a remarkably high CNS MPO score of 6.0.[15] Unexpectedly reversing the thiazole ring (**9**) or removing the substituent on position 2 (**4**) led to decreased PDE10A biological activity (data not shown).

Table 1. In vitro potency,[a] metabolic stability,[b] and permeability[14] of thiazolopyrazine derivatives.

Compds (Fig. 2)	hPDE10A IC_{50}, nM	Microsomal stability mCl, µL/min/mg human	rat	MDCK-MDR1 P_{app} (10E-6 cm/s)	ER
WEB-3	17	26	35	33	0.6
1	83			57	0.7
2	87	16	45	89	1.1
3	115	4	16	68	0.7
5	125	6	3	66	0.5
6	639	7	12	73	0.7
7	43	2	8	50	1
8	20	2	3	56	2

[a]hPDE10A IC_{50} were measured in *in vitro* enzymatic reaction using recombinant proteins and are means of at least two experiments (< 1µM).[10] Test - retest are within max. 2-fold.
[b]Microsomal intrinsic clearance values were determined according to literature procedures[16] and are means of at least two experiments.

In order to break the planarity and thus to avoid the potential risk of mutagenicity,[9] analogs **5**-**8** which carry a larger residue in position 8 were prepared (Table 1). Very sensitive SAR were observed when varying the C_8-substituent: IC_{50} vary from 43 nM to > 600nM for regioisomeric Me-pyridines while retaining the favorable DMPK profile of **3** (moderate microsomal stability, high P_{app} and low efflux ratio value supporting passive transport, Table 1). The replacement of *n*-Pr with large aromatic rings forces a shift in binding mode compared to WEB-3 (Fig. 5). The added aromatic rings can no longer be properly accommodated under residue Leu685. Instead, each of the new analogs is forced to find a novel binding spot, with various degrees of

complementarity with their respective microenvironments (dependent upon the proximity/distance from/to residue Leu685).[13] For example, Me at the *ortho* position (**7**) is still well tolerated because it is still away from Leu685 (Fig. 4). However, moving the Me substituent to the *meta* position (**5**), or even further out (to the *para* position, **6**), led to decreased PDE10A biological activity.

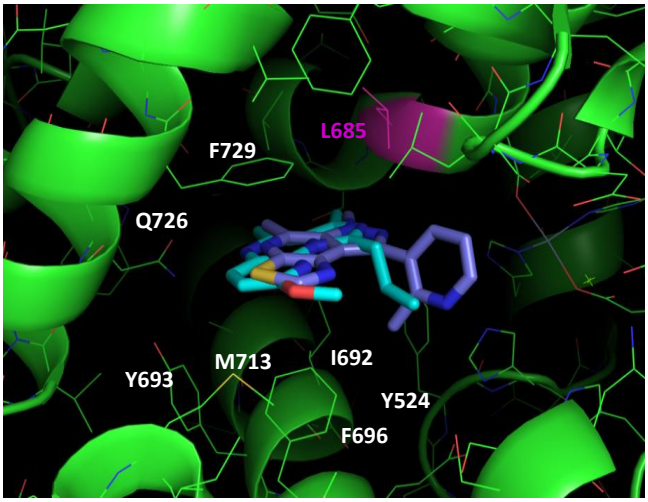

Figure 4. Comparison of **7** (purple) docked into the PDE10A protein (green) and WEB-3 (PDB: 3LXG, cyan) bound to the PDE10A binding site.[12] Notice the shift in binding as pyridine can no longer fit right beneath Leu685 (shown in magenta).

The 2-Me-pyridin-3-yl (in **7**) was thus preferred because it afforded an *in vitro* hPDE10A potency below 50nM, and an improved profile compared to WEB-3 (improved LLE (4.7) and *in vitro* DMPK properties (mCl & P_{app}), Table 1). A benzamide moiety was also tolerated (in **8**), as it was predicted to make a H-bond interaction with the side chain of proximal residue Ser581 (Fig. 5A).[12]

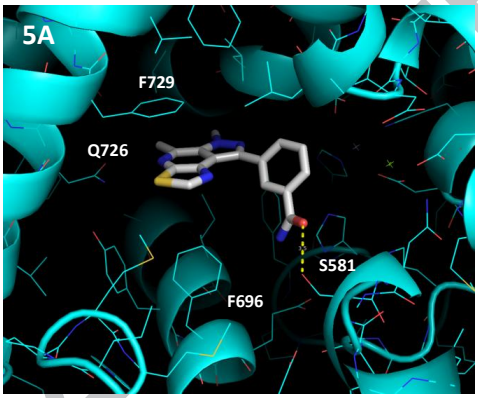

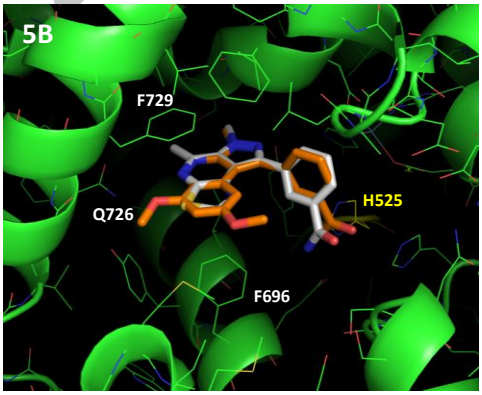

Figure 5. A) Model of **8** (white) docked into a model of the PDE10A protein (cyan). B) Comparison of **8** (white) and **29** (orange) manually docked into the PDE10A protein (green).[12]

8 constituted the front runner of this series; it combined low clogP (2.2), high TPSA (86), high LLE (5.5), single digit microsomal stability (human and rat, Table 1) and high permeability (P_{app} 56 10E-6 cm/s). However the PDE2A selectivity was sub-optimal (Table 2).

Table 2. PDE selectivity profile[a]. (thiazolopyrazine series)

Compds (Fig. 2)	hPDE10A IC_{50}, nM	hPDE2A IC_{50}, nM	hPDE3A IC_{50}, nM	hPDE4D2 IC_{50}, nM
WEB-3	17	2160	8500	5540
1	83	4890	16500	7850
2	87	3010	7070	1780
3	115		7840	4220
5	125		7850	4270
7	43	1860	7470	13500
8	20	1310	4940	2980

[a]hPDE10A, 2A, 3A & 4D2[8a] IC_{50} were measured in *in vitro* enzymatic reaction using recombinant proteins and are means of at least two experiments (< 1µM).[10] Test - retest are within max. 2-fold.

As no path was clear how to diminish PDE2A affinity while retaining or improving PDE10A potency,[17] we then turned our attention to a related chemical series which enclosed a cinnoline central core (Fig. 6).

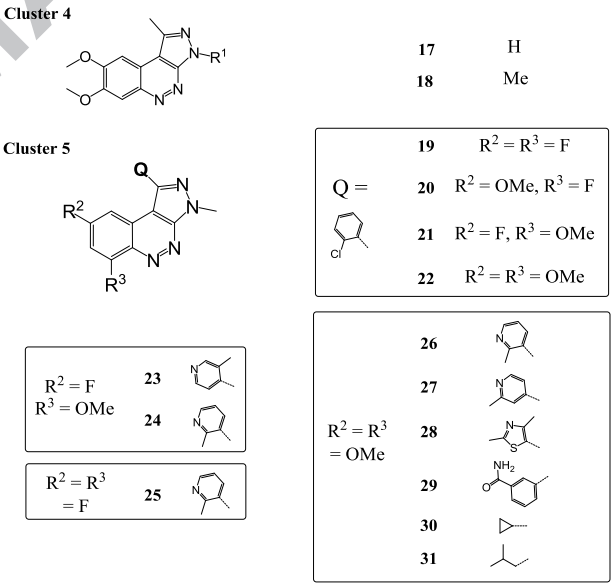

Figure 6. Cinnoline derivatives **17**-**31**

This second approach was suggested by the structural analogy of a HTS hit (**17**, cinnolines, Fig. 1) which combined good PDE10A *in vitro* potency (84nM, Table 3) and high selectivity towards PDE isoforms PDE4D2 & PDE2A (Table 4). *N*-methylation (position 3, **18**) impacted the CNS MPO score very favorably (from 3.8 to 5.0).

The HTS hit **17** was expected to be a good WEB-3 mimetic given the similarity in the overall 6,6,5 core structure with nitrogen acceptors at positions 2 and 6. The observed reduction in potency was attributed to the lack of elaboration of the core. However, upon crystal structure analysis, it was revealed that **17** has a different binding mode which is rotated 90° with respect to WEB-3 (**Fig. 7**). **17** binds in the same plane as WEB-3, making 2 H-bonds to Gln726 *via* the oxygens of the two methoxy groups,

one water mediated H-bond to Tyr524, and π-stacking interactions to Phe729 (above the plane).

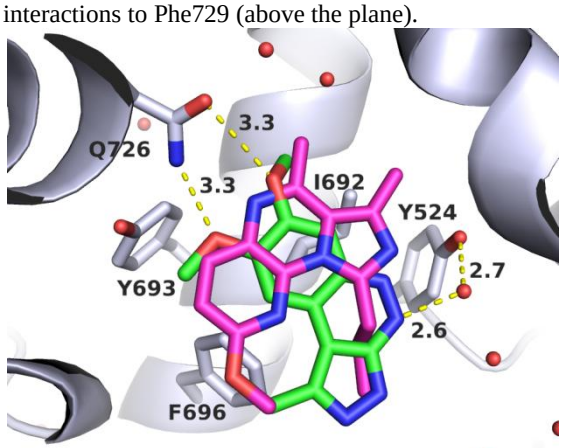

Figure 7. Superposition of WEB-3 (PDB: 3LXG, fushia) with **17** (green, PDB: 6MSA) bound to hPDE10a showing the 90° rotation of the core in the plane with respect to WEB-3. Key interacting residues are shown except for Phe729 which contributes π-stacking interactions from above the plane.

It can be seen from the overlay of the crystal structure of **23** and WEB-3 (**Fig. 8**), that elaboration of **17** at the 1 and 3 positions sucessfully rotates the core to be more closely aligned with WEB-3. However, the addition of the bulky aromatic ring at position 1 and the methoxy group at position 6 results in an overall shift of the molecule; the methyl pyrimidine is then positioned in a pocket just past Leu675: this enables the ring to adopt an orientation nearly perpendicular to the core while the methyl substituent fits into a small hydrophobic pocket between Phe696 and Tyr524. The oxygen of the 6-OMe makes the H-bond to Gln726 and the nitrogen at position 2 makes a water mediated H-bond to Tyr524.

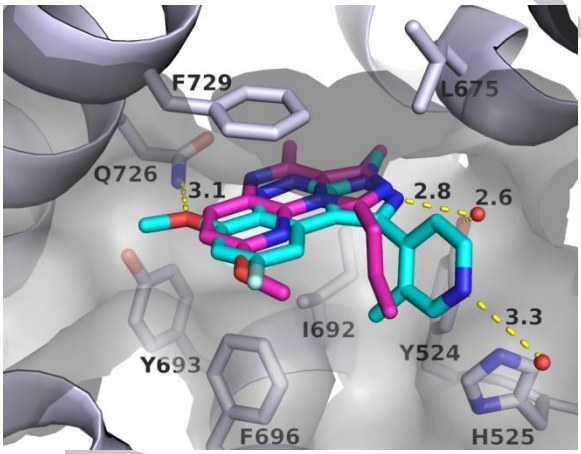

Figure 8. Superposition of WEB-3 (PDB: 3LXG, fushia) with **23** bound to hPDE10a (teal, PDB: 6MSC). Note that the core of **23** is shifted for the OMe to make the hydrogen bond to Q726; and in order to accommodate the methylpyrimidine in the pocket beneath L675, the methyl fits into the hydrophobic pocket formed by F696, I692, Y524 and H525.

Analogs **19-31** (Fig. 6, cluster 5) were prepared[11] starting from the corresponding commercially available phenylacetonitrile **32**. A pyrazole moiety was first built by intramolecular cyclization with methylhydrazine of the nitrile **34** and an acetate functionality introduced after benzylic metalation. Formation of the tricyclic cinnoline core could then be completed in presence of sodium nitrite (compound **35**). Finally the hydroxy group was activated to the triflate (**36**) which allowed Suzuki type coupling reactions to afford **19-31.**

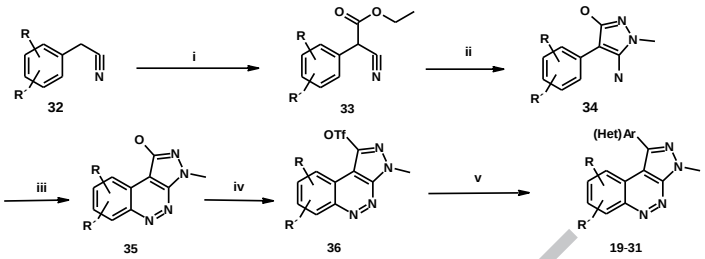

Scheme 2. Synthesis[11] of cinnoline derivatives: (i) diethyl carbonate, Na, 130°C; (ii) methylhydrazine, EtOH, 90°C; (iii) $NaNO_2$, HCl, 0°C to rt; (iv) Tf_2O, TEA, THF, -78°C to rt; (v) (Het)ArB$(OH)_2$, Pd$(Ph_3P)_4$, $NaHCO_3$, PhMe/EtOH: 4/1, 100°C or PdCl_2(dppf), Cs_2CO_3, dioxane/H_2O: 4/1, 100°C.

Starting from **18**, bulky residues (s. the discussion above for the thiazolopyrazine series) were introduced in position 1 in order to break the planarity and thus avoid potential mutagenicity.[9] We first focused our efforts on the optimization of the substitution pattern of the central core. A series of 2-Cl-phenyl derivatives carried by various 6,8-disubstituted cinnoline tricycles (**19-22**) was prepared;[18] we observed up to a 80-fold difference in PDE10A potency depending on the substituents: **19** *vs* **22**. Important learnings were gathered by one to one comparison of these four close analogs: a fluorine on position 6 is detrimental for *in vitro* PDE10A potency (**19** far less potent than its 6-OMe analog **21**) whereas both F and OMe are well tolerated on position 8 (compare **21** to **22**), possibly reflecting a combination of electronic and steric effects (i.e. electron-donating better than electron-withdrawing substituents, and superior complementarity of 6-OMe over F in a mixed lipophilic environment). Moreover, the OMe is nicely filling the pocket (VdW contacts and general hydrophobic interaction, not shown). Both **21** and **22** showed moderate PDE10A in vitro potency, high microsomal stability (human, hmCl <5 µL/min/mg) but high instability towards rat microsomes (rmCl > 200 µL/min/mg, Table 3).

Table 3. In vitro potency,[a] metabolic stability,[b] and permeability[14] of cinnoline derivatives. (**17-22**)

Compds (Fig. 6)	hPDE10A IC_{50}, nM	Microsomal stability mCl, µL/min/mg human	rat	MDCK-MDR1 P_{app} (10E-6 cm/s)	ER
WEB-3	17	26	35	33	0.6
17	84			63	1
18	171			60	0.8
19	1790	28	387	36	0.4
20	298			46	0.7
21	25	4	411	54	0.5
22	23	5	194	44	0.8

[a,b] *cf*. table 1.

In terms of selectivity towards other PDE isoforms high selectivity was achieved (>800-fold, Table 4) *versus* PDE3A and 4D2; unexpectedly, whereas the PDE2A selectivity was sub-optimal for **21** it was high for **22** (Table 4).

Table 4. PDE selectivity profile[a]. (cinnoline series)

Compds (Fig. 6)	hPDE10A IC_{50}, nM	hPDE2A IC_{50}, nM	hPDE3A IC_{50}, nM	hPDE4D2 IC_{50}, nM
WEB-3	17	2160	8500	5540
17	84	>100000	1110	>20000
18	171		>20000	>20000
21	25	923	>20000	>20000
22	23	12900	>20000	>20000
23	21	3520	8520	9540
24	83	5390	111900	14200
26	5	1320	23600	8920
27	105			6130

28	11		4270

[a] *cf.* table 2.

Analogs of **21** and **22** were prepared with a focus on lowering the lipophilicity; for both **21** and **22**, clogP was unfavorable (>4) leading to low LLE (3.4 and 3.1 resp.). Published SAR in related structural series[9] allowed us to expedite optimization by limiting our efforts to a short list of Me-pyridine analogs (**23**, **24**, and **26**).[19] **23** & **26** combined high CNS MPO score (>5.5), high LLE (5.2 and 5.5, resp.), moderate microsomal stability (h and r, table 5) and high permeability (Table 5). According to modeling, electron-withdrawing substituents on the phenyl ring of the tricyclic core (**25**) are less well tolerated than electron-donating groups in that ring (**23** and **24**), diminishing the pi-stacking and pi-facing strength of the core (not shown).

Table 5. In vitro potency,[a] metabolic stability,[b] and permeability[14] of cinnoline derivatives (**23**-**31**).

Compds (Fig. 6)	hPDE10A IC_{50}, nM	Microsomal stability mCl, µL/min/mg human	rat	MDCK-MDR1 P_{app} (10E-6 cm/s)	ER
23	21	6	8	53	0.8
24	83	4	7	68	0.7
25	1590	1	4	29	0.6
26	5	2	6	55	1
27	105				
28	11	2	27	57	1.1
29	555	5	164	38	9.6
30	535	4	8	62	0.8
31	1800				

[a,b] *cf.* table 1.

A few more analogs were prepared (Fig. 6, Table 5):

- examplarily a non-pyridine derivative was synthesized (**28** carries a diMe-thiazole in position 1): compared to **22**, LLE (4.6) and CNS MPO score (4.8) were improved; rmCl though lowered remained sub-optimal and higher compared to the one measured for **26** (Table 5); in this series, clogP was a good predictor of rmCl (clogP **22** 4.5, **23** 3.3, **26** 2.8);
- unlike what was observed in the thiazolopyrazine series (**8**), a benzamide in position 1 was detrimental for PDE10A *in vitro* potency (**29**, IC_{50} 555nM, Table 5); indeed, to avoid an intramolecular steric clash between the OMe and the benzamide groups of **29**, the benzamide moiety moves out, but becomes suboptimally close to residue His525 (Fig. 5B). The penalty results in much lower affinity for **29** compared to **8**;
- finally, we confirmed (with **25**) the negative impact on the affinity for PDE10A of the diF-substitution in presence of a pyridyl moiety in position 1; as discussed for **19** (above), replacing electron-donating moieties (OMe) by electron-withdrawing groups (F) disfavors pi-pi-interactions;
- our attempt to break the planarity with a cycloalkyl (3**0**, cyclopropyl) or branched alkyl (**31**, isobutyl) residue was not further pursued: despite increased f_{sp}^3, lower MW and retained high CNS MPO score (4.7 – 5.0), this approach was detrimental in term of PDE10A *in vitro* potency (IC_{50} > 500nM, Table 5). The diminished potency here might be reflective of the limited room available; in particular branched/substituted aliphatic groups might not accommodate this crowded region of the binding pocket.

When comparing to other tricyclic PDE10A inhibitors [such as imidazo[1,5-a]quinoxalines[9a] and benzo[e]imidazo[5,1-c][1,2,4]triazines[9b]], the 3H-pyrazolo[3,4-c]cinnolines (**23** & **26**) presented here have lowered clogP (2.5 and 2.8, resp.).[20] Furthermore based on their balanced and favorable *in vitro* profile **23** and **26** were advanced to rat PK (Table 6). Their improved microsomal stability (compared to WEB-3 data) translated to a much lower clearance *in vivo*. Their decreased clogP also translated to a decreased volume of distribution (Vss). **26** exhibited a shorter half-life but an improved bioavailability versus both **23** and WEB-3. While WEB-3 showed a higher brain/plasma ratio, both **23** and **26** showed around 10-fold increased dose-normalized free brain concentration at 1 hour post intraperitoneal administration; **23** and **26** have thus the potential to inhibit the PDE10A target *in vivo* at a lower efficacious dose than WEB-3.

Table 6. Pharmacokinetic profile in rat of **WEB-3, 23 & 26**

	WEB-3	**23**[21]	**26**[21]
clogP / TPSA / pKa	3.7 / 52 / 6.7	2.5 / 66 / 4.2	2.8 / 75 / 5.0
CNS MPO	5.2	5.5	5.7
LLE / $LigE^{lit}$	4.1 / 0.53	5.2 / 0.44	5.5 / 0.45
fu pl / fu br	0.003 / 0.007	0.097 / 0.094	0.032 / 0.068
$t_{1/2}$ (h) [a]	1.7	1.7	0.8
V_{SS} (L/kg) [a]	2.4	1.0	0.4
Cl_P (L/h/kg) [a]	2.6	1.2	1.0
F_{oral} (%) [b]	19	12	42
C (ng/ml, tot.) plasma / brain [c]	72 / 118	145 / 93	741 / 90
C (ng/ml, free) plasma / brain [d]	0.10 / 0.40	7 / 5	24 / 6
Brain : Plasma Ratio [c] (tot/free)	1.67 / 3.81	0.64 / 0.62	0.12 / 0.26

[a] After intravenous administration[e]
[b] After oral administration[e]
[c] After intraperitoneal administration[e], at 1 hour post-dosing
[d] Dose normalized
[e] iv, po, ip dose: 2 mg·kg^{-1} WEB-3 & **23**; 1 mg·kg^{-1} **26**.

In summary, novel phosphodiesterase 10A inhibitors were disclosed. In particular, optimization of a HTS hit (**17**) resulted in potent, selective and brain penetrant **23** and **26**; both exhibited much lower clearance *in vivo* and decreased volume of distribution (rat PK) and have thus the potential to inhibit the PDE10A target *in vivo* at a lower efficacious dose than WEB-3.

Declaration of Interest

The authors declare the following competing financial interest(s): The authors are current or former employees of AbbVie, and may own company stocks; the design, study conduct, and financial support for this research were provided by AbbVie. AbbVie participated in the interpretation of data, review, and approval of the publication. [$]K.D. is a former AbbVie employee.

Acknowledgments

We would like to thank Ferdinand Regner and Sonja Triebel and the Analytical Chemistry group in Ludwigshafen. Use of the IMCA-CAT beamline 17-ID at the Advanced Photon Source was supported by the companies of the Industrial Macromolecular Crystallography Association through a contract with Hauptman-Woodward Medical Research Institute. Use of the Advanced Photon Source was supported by the U.S. Department of Energy, Office of Science, Office of Basic Energy Sciences, under Contract No. DE-AC02-06CH11357.

References and notes

1. Siuciak, J.A.; McCarthy, S.A.; Chapin, D.S.; Martin, A. N. *Psychopharmacol.* **2008**, *197*, 115.
2. Rodefer, J.S; Murphy, E.R.; Baxter, M.G. *Eur. J. Neurosci*. **2005**, *4*, 1070.
3. Kehler, J.; Kilburn, J.P. *Exp. Opin Ther. Pat.* **2009**, *19*, 1715.

4. U.S. Patent 2005/0202550 A1, 2005. Chem. Abstr. 2005, 143, 301347.
5. Verhoest, P.R.; Chapin, D.S.; Corman, M.; Fonseca, K.; Harms, J.F.; Hou, X.; Marr, E.S.; Menniti, F.S.; Nelson, F.; O'Connor, R.; Pandit, J.; Proulx-Lafrance, C.; Schmidt, A.W.; Schmidt, C.J.; Suiciak, J.A.; Liras, S. *J. Med. Chem.* **2009**, **52**, 5188.
6. Hoefgen, N.; Stange, H.; Schindler, R.; Lankau, H.-J.; Grunwald, C.; Langen, B.; Egerland, U.; Tremmel, P.; Pangalos, M.N.; Marquis, K.L.; *et al*. *J. Med. Chem.* **2010**, *53*, 4399.
7. Advanced candidates include (a) MP-10 (PF-2545920, Pfizer).[5] (b) OMS-824 (Omeros), Cutshall, N.S.; Onrust, R.; Rohde, A.; Gragerov, S.; Hamilton, L.; Harbol, K.; Shen, H.R.; McKee, S.; Zuta, C.; Gragerova, G.; Florio, V.; Wheeler, T.N.; Gage, J.L. *Bioorg. Med. Chem. Lett.* **2012**, *22*, 5595. (c) AMG-579 (Amgen), Hu, E.; Chen, N.; Bourbeau, M.P.; Harrington, P.E.; Biswas, K.; Kunz, R.K.; Andrews, K.L.; Chmait, S.; Zhao, X.; Davis, C.; Ma, J.; Shi, J.; Lester-Zeiner, D.; Danao, J.; Able, J.; Cueva, M.; Talreja, S.; Kornecook, T.; Chen, H.; Porter, A.; Hungate, R.; Treanor, J.; Allen, J.R. *J. Med. Chem.* **2014**, *57*, 6632. (d) PBF-999 (Palobiofarma), ClinicalTrials.gov Identifier: NCT02907294. (e) TAK-063 (Takeda), Kimura, H.; Taniguchi, T.; *Med. Chem. Rev*. **2017**, *52*, 3. (f) RG-7203 (Roche) and FRM-6308 (Forum) Thomson Reuters Cortellis Web site, https://cortellis.thomsonreuterslifesciences.com.
8. (a) In particular selectivity towards PDE2A, 3A & 4D2 is critical; for that reason these 3 PDEs were selected as our entry selectivity panel. PDE2 is known to play a role in schizophrenia, PDE3 inhibition might induce CV side effects and we had PDE4 cross activity with earlier structural series; (b) The *in vitro Salmonella* Bacterial Reverse Mutation Assay or Mini-Ames Test is a widely used short-term genotoxicity assay for the detection of gene mutations. The plate incorporation assay uses histidine-dependent *Salmonella* tester strains TA98 and TA100 and is carried out in the absence and presence of an exogenous metabolic activation system (S9). A test article that produces a response with the highest increase equal to or exceeding twice the vehicle control value and with a concentration-related increase is considered mutagenic.
9. (a) Malamas, M.S.; Ni, Y.-K.; Erdei, J.; Stange, H.; Schindler, R.; Lankau, H.-J.; Grunwald, C.; Fan, K.Y.; Parris, K.; Langen, B.; et al. *J. Med. Chem.* **2011**, *54*, 7621. (b) Malamas, M.S.; Stange, H.; Schindler, R.; Lankau, H.-J.; Grunwald, C.; Langen, B.; Egerland, U.; Hage, T.; Ni, Y.; Erdei, J.; *et al*. *Bioorg. Med. Chem. Letters* **2012**, *22*, 5876.
10. The preparation of the building blocks mentioned, typical procedures, and assay setup are described in WO 2014041175, 2014. Chem. Abstr. 2014, 160, 487023, and references cited therein.
11. The preparation of the building blocks mentioned, typical procedures, and assay setup are described in WO 2014027078, 2014. Chem. Abstr. 2014, 160, 341156, and references cited therein.
12. (a) Models were generated using Schrodinger software, Release 2018-1, and figures were prepared using the PyMOL Molecular Graphics System, Version 2.0 Schrödinger, LLC. (b) Li, J.; Chen, Y.-L.; Deng, Y.-L.; Zhou, Q.; Wu, Y.; Wu, D.; Luo, H.-B. *Front. Chem.* **2018**, *6*, 167.
13. LLE (or LipE) = −log Ki − clogP. (a) Leeson, P. D.; Springthorpe, B. *Nat. Rev. Drug Discov*. **2007**, *6*, 881. (b) Hopkins, A. L.; Groome, C. R.; Alex, A. *Drug Discov. Today* **2004**, *9*, 430. LigE (or LE) Bembenek, S.D.; Tounge, B.A.; Reynolds, C.H. *Drug Discov. Today* **2009**, *14*, 278.
14. MDCK-MDR1 human P-gp transfected cell line - P_{app} = apparent permeability, compound flux across cell monolayer in Transwell system, either in direction apical-to-basolateral (AB) or vice versa (BA); ER = Efflux Ratio = Ratio of P_{app} values BA/AB; Passive perm = P_{app} AB in the presence of a pan-transporter inhibitor.
15. Wager, T.T.; Hou, X.; Verhoest, P.R.; Villalobos, A. *ACS Chem. Neurosci.* **2010**, *1*, 435.
16. Obach, S. *Drug Metab. Dispos.* **1999**, *27*, 1350.
17. PDE2 and PDE10 are quite conserved overall, with high residue conservation around the binding site: Omori, K.; Kotera, J. *Circul. Res.* **2007**, *100*, 309.
18. This effort could be expedited by published SAR in related structural series.[9b]
19. Synthesis of the 2-Me-4-pyridine analog of **22** failed.
20. s. front runners **96**[9a] & **106**[9a] (clogP ≥ 4.3), **53**[9b] (clogP 3.3); logP are calculated using Biobyte calculator.
21. analytical data **23** ESI MS (HRMS, m/z): calcd for $C_{17}H_{15}FN_5O$ 324.13, found 324.13 [M + H^+]; ^{1}H-NMR (400 MHz, d6-DMSO) δ (ppm) = 8.76 (s, 1H), 7.36 (d, J= 4.8 Hz, 1H), 7.55 (d, J=4.8 Hz, 1H), 7.32 (dd, J=l 1.6, 2.4 Hz, 1H), 6.75 (dd, J=l 1.6, 2.4 Hz, 1H), 4.50 (s, 3 H), 4.15 (s, 3 H), 2.20 (s, 3 H); ^{13}C-NMR (126 MHz, DMSO) δ 166.48, 164.47, 160.83, 160.72, 150.26, 146.69, 142.96, 139.35, 135.80, 135.63, 127.19, 122.51, 122.40, 107.38, 99.61, 99.38, 97.86, 97.66, 57.55, 35.91, 17.10; **26** ESI MS (HRMS, m/z): calcd for $C_{18}H_{18}N_5O_2$ 336.15, found 336.15 [M + H^+]; ^{1}H-NMR (400 MHz, d6-DMSO) δ (ppm) = 8.68-8.66 (m, 1H), 7.94-7.92 (m, 1H), 7.48-7.45 (m, 1H),6.89 (d, J= 2.0 Hz 1 H), 6.39 (d, J= 2.0 Hz 1 H), 4.45 (s, 3 H), 4.08 (s, 3 H), 3.70 (s, 3 H), 2.39 (s, 3 H); kinome profiling (**23** & **26**): IC_{50} > 10μM for >80 kinases, ATP compet. binding; mini-Ames Test[8b] (**23** & **26**): negative; hERG (QPatch, HEK293, human): **23** (IC_{50} 17.3 μM), **26** (IC_{50} >30 μM).

Graphical Abstract

To create your abstract, type over the instructions in the template box below.
Fonts or abstract dimensions should not be changed or altered.

Novel, potent, selective, and brain penetrant phosphodiesterase 10A inhibitors

Leave this area blank for abstract info.

Hervé Geneste*, Karla Drescher, Clarissa Jakob, Loïc Laplanche, Michael Ochse, Maricel Torrent

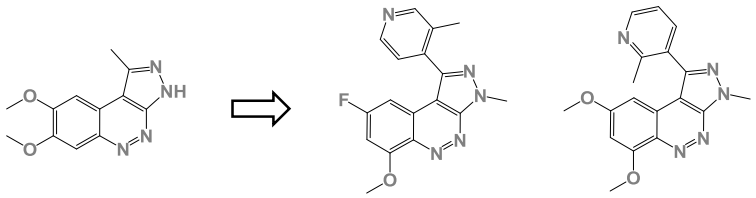

- optimization supported by x-ray crystal structure analysis and molecular modeling
- **23** and **26**: potent, selective, and brain penetrant
- improved PK profile (rat): lower clearance in vivo and decreased volume of distribution (compared to WEB-3)

Ms. No.: BMCL-D-18-01566
Title: Novel, potent, selective, and brain penetrant phosphodiesterase 10A inhibitors
Corresponding Author: Dr. Hervé Geneste
Authors: Karla Drescher, Clarissa Jakob, Loïc Laplanche, Michael Ochse, Maricel Torrent

Highlights

- novel PDE10 inhibitors
- optimization supported by x-ray crystal structure analysis and molecular modeling
- potent, selective, and brain penetrant
- improved PK profile (rat): lower clearance *in vivo* and decreased volume of distribution (compared to WEB-3)